Doa4 function in ILV budding is restricted through its interaction with the Vps20 subunit of ESCRT-III

Caleb M. Richter, Matthew West and Greg Odorizzi*

Molecular, Cellular, and Developmental Biology, University of Colorado, Boulder, CO 80309, USA

*Author for correspondence (odorizzi@colorado.edu)

Accepted 23 January 2013
Journal of Cell Science 126, 1881–1890

doi: 10.1242/jcs.122499

Summary

Assembly of the endosomal sorting complex required for transport (ESCRT)-III executes the formation of intralumenal vesicles (ILVs) at endosomes. Repeated cycles of ESCRT-III function requires disassembly of the complex by Vps4, an ATPase with a microtubule interaction and trafficking (MIT) domain that binds MIT-interacting motifs (MIM1 or MIM2) in ESCRT-III subunits. We identified a putative MIT domain at the N-terminus of Doa4, which is the ubiquitin (Ub) hydrolase in *Saccharomyces cerevisiae* that deubiquitinates ILV cargo proteins. The Doa4 N-terminus is predicted to have the α-helical structure common to MIT domains, and it binds directly to a MIM1-like sequence in the Vps20 subunit of ESCRT-III. Disrupting this interaction does not prevent endosomal localization of Doa4 but enhances the defect in ILV cargo protein deubiquitination observed in cells lacking Bro1, which is an ESCRT-III effector protein that stimulates Doa4 catalytic activity. Deletion of the *BRO1* gene (*bro1Δ*) blocks ILV budding, but ILV budding was rescued upon disrupting the interaction between Vps20 and Doa4. This rescue in ILV biogenesis requires Doa4 expression but is independent of its Ub hydrolase activity. Thus, binding of Vps20 to the Doa4 N-terminus inhibits a non-catalytic function of Doa4 that promotes ILV formation.

Key words: Multivesicular body, Vesicle budding, Deubiquitination

Introduction

The endosomal sorting complexes required for transport (ESCRTs) sort ubiquitinated transmembrane proteins at endosomes into intralumenal vesicles (ILVs) that are subsequently degraded in the hydrolytic interior of lysosomes upon endolysosomal fusion. ILV cargo recognition is mediated by ESCRT-0, -I, and -II, which bind directly to ubiquitin (Ub) conjugates on the cytosolic domains of transmembrane proteins targeted for destruction (reviewed in Henne et al., 2011). Based on *in vitro* studies that reconstituted ILV budding at synthetic membranes, ESCRT-I and -II induce the formation of ILV buds that detach as free ILVs upon membrane scission catalyzed by ESCRT-III (Wollert and Hurley, 2010; Wollert et al., 2009). How the activities of ESCRTs are regulated *in vivo* to drive the ILV budding reaction is poorly understood.

ESCRT-III subunits exist as soluble inactive monomers and polymerize into the active complex only on membranes (Babst et al., 2002; Shim et al., 2007), which is a prerequisite to execute membrane scission (Wollert et al., 2009). *Saccharomyces cerevisiae* has seven ESCRT-III subunits, four of which (Vps20, Snf7, Vps24 and Vps2) are thought to comprise the core of the complex and assemble in the above order (Teis et al., 2008). Vps20 initiates ESCRT-III assembly by stimulating homopolymerization of Snf7, the most abundant subunit of the complex (Saksena et al., 2009; Teis et al., 2008). Vps24 and Vps2 terminate ESCRT-III assembly by capping the Snf7 polymer (Teis et al., 2008). The other ESCRT-III subunits (Did2, Ist1 and Vps60) regulate disassembly of the complex but are not strictly required for ILV budding (Dimaano et al., 2008; Nickerson et al., 2006; Rue et al., 2008).

Vps4 catalyzes disassembly and dissociation of ESCRT-III subunits from the membrane, which is essential to recycle subunits for subsequent rounds of complex assembly. Vps4 belongs to the diverse family of AAA+ ATPases that unfold proteins and/or disassemble protein complexes (Babst et al., 1998). Direct contact between Vps4 and ESCRT-III is mediated by the microtubule interacting and trafficking (MIT) domain at the N-terminus of Vps4, which binds two distinct MIT-interacting motifs (MIM1 or MIM2) at or near the C termini of ESCRT-III subunits (Kieffer et al., 2008; Obita et al., 2007; Stuchell-Brereton et al., 2007). The MIT domain of Vps4 binds every ESCRT-III subunit through either its MIM1 (in Vps24, Vps2, Did2 and Ist1) or MIM2 (in Vps20, Snf7 and Ist1). However, other ESCRT-III effector proteins that contain MIT domains bind more selectively to a single subunit or subset of subunits (reviewed in Hurley, 2010), including AMSH and UBPY, two Ub hydrolases in humans that bind a distinct but overlapping subset of ESCRT-III proteins (Agromayor and Martin-Serrano, 2006; Row et al., 2007).

In yeast, two MIT domains exist in Vta1 (Xiao et al., 2008), which is a Vps4 cofactor that stimulates its ATPase activity (Azmi et al., 2006; Azmi et al., 2008; Lottridge et al., 2006), but no other yeast proteins that associate with ESCRT-III are known to have an MIT domain. We show that the yeast Doa4 Ub hydrolase contains a candidate MIT domain at its N-terminus that interacts specifically with Vps20. Binding to the Doa4 N-terminus requires conserved amino acids within a MIM1-like sequence in helix α6 at the C terminus of Vps20. This site, which we refer to as MIMα6, is spatially separate from the MIM2 sequence in Vps20 that binds the MIT domain of Vps4 (Kieffer

et al., 2008; Shestakova et al., 2010). Mutation of Vps20 MIMα6 (*vps20*$^{\Delta MIM\alpha6}$) alone did not impair Doa4 function, but the *vps20*$^{\Delta MIM\alpha6}$ mutation caused a strong synthetic inhibition of deubiquitination when combined with deletion of the *BRO1* gene, which encodes an ESCRT-III-associated protein that stimulates Doa4 Ub hydrolase activity (Richter et al., 2007). Surprisingly, the *vps20*$^{\Delta MIM\alpha6}$ mutation rescued ILV budding in the absence of Bro1, and this rescue required Doa4 expression but was independent of Doa4 Ub hydrolase activity. These results reveal an unexpected non-catalytic role for Doa4 in ILV budding that is inhibited through its interaction with the Vps20 subunit of ESCRT-III.

Results

The N-terminus of Doa4 binds a MIM1-like sequence in Vps20 helix α6

The Snf7 subunit of ESCRT-III in yeast binds Bro1 (Kim et al., 2005; Odorizzi et al., 2003), which is an auxiliary protein that stabilizes ESCRT-III assembly (Wemmer et al., 2011). Bro1 also functions as an ESCRT-III effector by promoting the deubiquitination of ILV cargoes through its recruitment and activation of Doa4 (Luhtala and Odorizzi, 2004; Richter et al., 2007). Deubiquitination by Doa4 is required for cargoes to be sorted into ILVs (Nikko and André, 2007), and the need for Bro1 in Doa4 function can be bypassed by overexpressing the *DOA4* gene (Amerik et al., 2006; Luhtala and Odorizzi, 2004). Deleting *BRO1* (*bro1Δ*) in tandem with other ESCRT genes revealed that each of the core ESCRT-III subunits (Snf7, Vps20, Vps2 or Vps24) is required for overexpressed Doa4-GFP to localize to endosomes in the absence of Bro1 (Fig. 1). In addition, ESCRT-III subunits co-immunoprecipitated with Doa4-GFP overexpressed from a high-copy (2μ) plasmid regardless of whether *BRO1* was deleted (Fig. 2A), indicating that Doa4 associates with ESCRT-III independently of Bro1, provided that the ESCRT-III core complex is intact.

Amino acids 1-80 of Doa4 are predicted to fold into three α helices (Fig. 2B), which is similar to the size and secondary structure of MIT domains in Vps4 and Vta1 (Obita et al., 2007; Xiao et al., 2008). Therefore, we hypothesized Doa4 residues 1-80 comprise an MIT-like domain lacking sequence homology to the known MIT domains that mediate binding of Vps4 and Vta1 to ESCRT-III subunits (Kieffer et al., 2008; Obita et al., 2007; Stuchell-Brereton et al., 2007; Xiao et al., 2008). In support of this hypothesis, purified recombinant GST-Doa4$^{1\text{-}80}$ bound HA-tagged Vps20 (Fig. 2C), and this interaction was abolished by mutation of conserved residues in Vps20 helix α6 that are similar to the MIM1 consensus sequence that binds the Vps4 MIT domain (Fig. 2D; Obita et al., 2007). Like the MIT domains of human AMSH and UBPY (Agromayor and Martin-Serrano, 2006; Row et al., 2007), the N-terminus of Doa4 exhibits binding specificity because GST-Doa4$^{1\text{-}80}$ did not bind other core ESCRT-III subunits, Vps2, Snf7 or Vps24 (Fig. 2C).

Vps20 MIMα6 is not required for Doa4 endosomal recruitment

Endosomal localization of Doa4 is disabled by mutations within residues 1-80 (Amerik et al., 2006), raising the possibility that endosomal recruitment of Doa4 is mediated by its interaction with the MIM1-like sequence in Vps20 helix α6 (hereafter

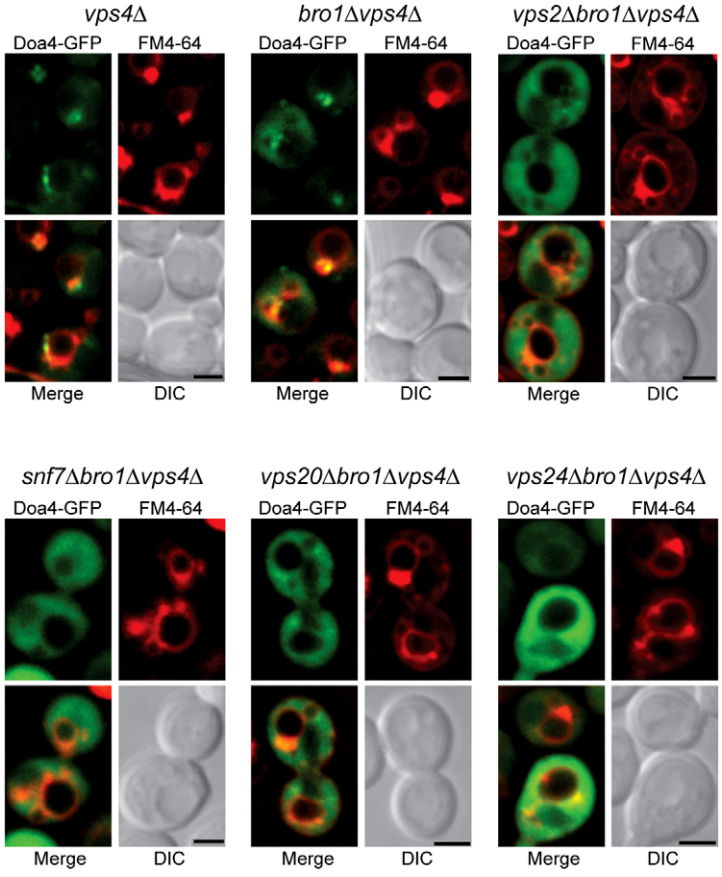

Fig. 1. ESCRT-III is required for Bro1-independent localization of overexpressed Doa4 to endosomes. Fluorescence and differential interference contrast (DIC) microscopy of 2μ Doa4-GFP and FM4-64, a fluorescent dye that labels class E compartments and vacuolar membranes (Vida and Emr, 1995). Scale bars: 2 μm.

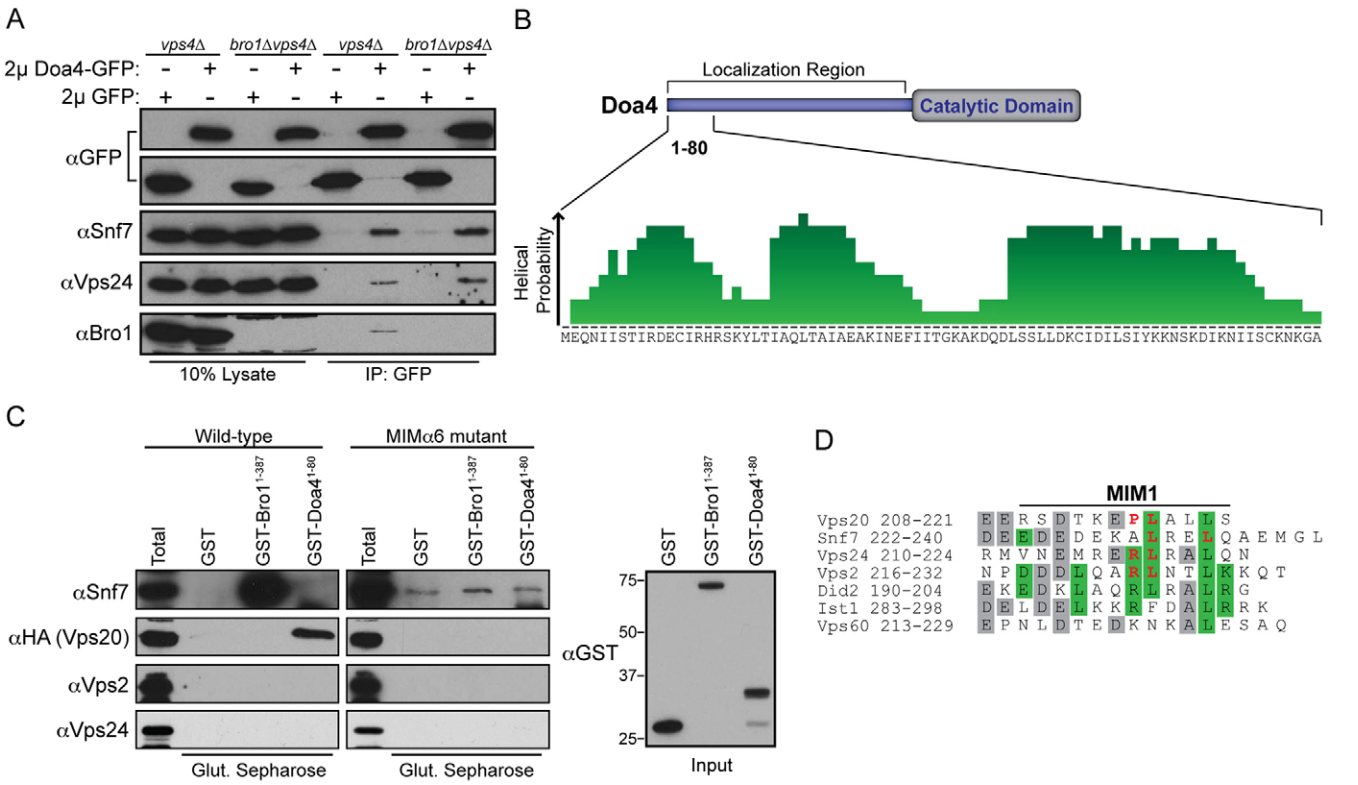

Fig. 2. The N-terminal domain of Doa4 binds to a MIM1-like sequence in Vps20 helix α6. (**A**) *In vivo* αGFP immunoprecipitation (IP) of 2μ GFP or Doa4-GFP and immunoblot with αGFP, αSnf7, αVps24 and αBro1. The experiment was performed in *vps4Δ* cells to stabilize ESCRT-III, which is largely disassembled at steady state in the presence of *VPS4*. (**B**) PredictProtein (Rost et al., 2004) helical probability plot for amino acids 1-80 of Doa4. (**C**) *In vitro* glutathione (Glut.)–Sepharose pulldowns of purified GST, GST-Bro1$^{1\text{-}387}$, or GST-Doa4$^{1\text{-}80}$ mixed with *E. coli* lysates expressing wild-type or MIMα6-mutant Snf7, Vps20-HA, Vps2, or Vps24. GST-Bro1$^{1\text{-}387}$ served as a positive control for binding to the α6 helix of Snf7. For unknown reasons, the MIMα6 mutant of Snf7 had a higher propensity for non-specific binding than wild-type Snf7. Immunoblots were probed with αSnf7, αHA, αVps2, αVps24 or αGST. (**D**) Sequence alignment of the α6 helices of *S. cerevisiae* ESCRT-III subunits using the PredictProtein online server (Rost et al., 2004), which contain MIM1 or MIM1-like sequences. Grey boxes indicate conserved residues and green boxes indicate residues that conform to the MIM1 consensus sequence (D/E)xxLxxRLxxL(K/R). Red lettering designates the positions at which the endogenous residues were substituted with aspartic acid in the MIMα6 mutants in C.

referred to as Vps20 MIMα6). However, unlike full-length Doa4-GFP (Luhtala and Odorizzi, 2004; Fig. 3), GFP-Doa4$^{1\text{-}80}$ exhibited a predominantly cytosolic distribution rather than the punctate localization characteristic of endosomes (Fig. 3). GFP-Doa4$^{1\text{-}80}$ was similarly cytosolic in *vps4Δ* cells (Fig. 3), which provided more compelling evidence that the N-terminus of Doa4 cannot autonomously mediate endosomal recruitment because the absence of Vps4 traps wild-type Doa4 at aberrant endosomal structures known as 'class E compartments' formed in ESCRT-mutant strains (Luhtala and Odorizzi, 2004; Fig. 3). Curiously, GFP-Doa4$^{1\text{-}80}$ was present occasionally within the vacuole lumen of wild-type cells (Fig. 3), suggesting it had been packaged into ILVs bound for vacuolar delivery because of transient association with ESCRT-III.

Further evidence that endosomal recruitment of Doa4 is not mediated by interaction of its N-terminus with Vps20 came from our analysis of cells expressing the *vps20*$^{\Delta MIM\alpha6}$ allele, in which the conserved residues essential for binding of Vps20 to Doa4$^{1\text{-}80}$ were mutated (Fig. 2D). The *vps20*$^{\Delta MIM\alpha6}$ mutation did not disable localization of full-length Doa4-GFP to endomembranes either in wild-type or *vps4Δ* cells (Fig. 3). Nonetheless, the Doa4 N-terminus might be required in the context of a larger localization determinant because deletion of residues 1-80 blocked the accumulation of Doa4-GFP at class E compartments in *vps4Δ* cells (Fig. 3).

Mutation of Vps20 MIMα6 causes dominant-synthetic inhibition of deubiquitination

The ATPase activity of Vps4 is stimulated by interaction of its MIT domain with MIMs in ESCRT-III subunits (Merrill and Hanson, 2010; Obita et al., 2007; Stuchell-Brereton et al., 2007). We investigated whether the Ub hydrolase activity of Doa4 is similarly stimulated by interaction of its N-terminal domain with MIMα6 in Vps20. Direct *in vitro* assay of Doa4 catalytic activity in response to binding of its N-terminus was complicated by difficulties in purifying full-length recombinant Doa4 (data not shown). However, Doa4 activity can be monitored *in vivo* by assaying the abundance of ubiquitinated Cps1, which is a transmembrane protein deubiquitinated by Doa4 prior to its enclosure within ILVs (Dupré and Haguenauer-Tsapis, 2001; Katzmann et al., 2001; Reggiori and Pelham, 2001). Because Bro1 stimulates Doa4 catalytic activity, Cps1 accumulates in its ubiquitinated form (Ub-Cps1) in *bro1Δ* cells (Richter et al., 2007; Fig. 4A). Introduction of the *vps20*$^{\Delta MIM\alpha6}$ mutation in *bro1Δ* cells further increased the accumulation of Ub-Cps1, but cells harboring the *vps20*$^{\Delta MIM\alpha6}$ mutation alone had no apparent

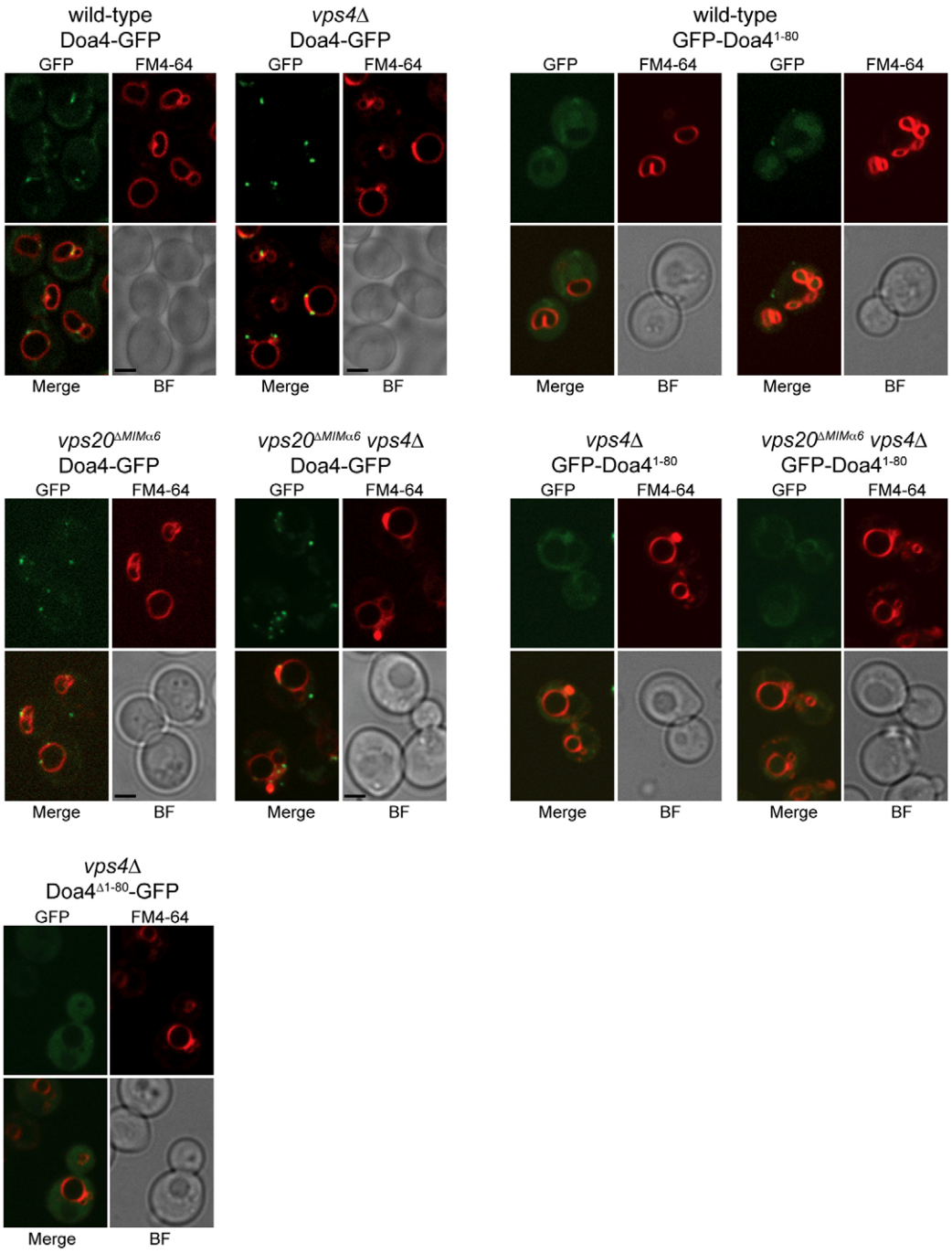

Fig. 3. Vps20 MIMα6 does not recruit Doa4 to endomembranes. Fluorescence and brightfield (BF) microscopy of Doa4-GFP, GFP-Doa4$^{1-80}$, or Doa4$^{\Delta 1-80}$-GFP and FM4-64. Scale bars: 2 μm.

defect in Cps1 deubiquitination (Fig. 4A). Enhancement of the Cps1 deubiquitination defect in *bro1Δ* cells did not occur upon simultaneous deletion of the entire *VPS20* gene. Instead, the abundance of Ub-Cps1 both in *vps20Δ* cells and in *vps20Δ bro1Δ* cells was similar to that in *bro1Δ* cells (Fig. 4A), consistent with the epistatic relationship Vps20 has in initiating ESCRT-III assembly for subsequent recruitment of Bro1 and Doa4 (Saksena et al., 2009; Teis et al., 2008). The dominant-synthetic inhibition of Cps1 deubiquitination seen when the *vps20*$^{\Delta MIM\alpha 6}$ and *bro1Δ* mutations were combined was mirrored in the analysis of total polyubiquitin conjugates from cell extracts, which accumulated to a greater extent in *bro1Δ* cells when the *vps20*$^{\Delta MIM\alpha 6}$ mutation was introduced (Fig. 4B). That the accumulation of total polyubiquitin conjugates in *vps20*$^{\Delta MIM\alpha 6}$ *bro1Δ* was less pronounced than the accumulation of Ub-Cps1 might be due to the abundance of cellular proteins that do not rely on Doa4 for deubiquitination, whereas Doa4 is the primary Ub hydrolase for Cps1.

The results described above suggest that Vps20 functions in parallel with Bro1 to activate Doa4 catalytic activity. However,

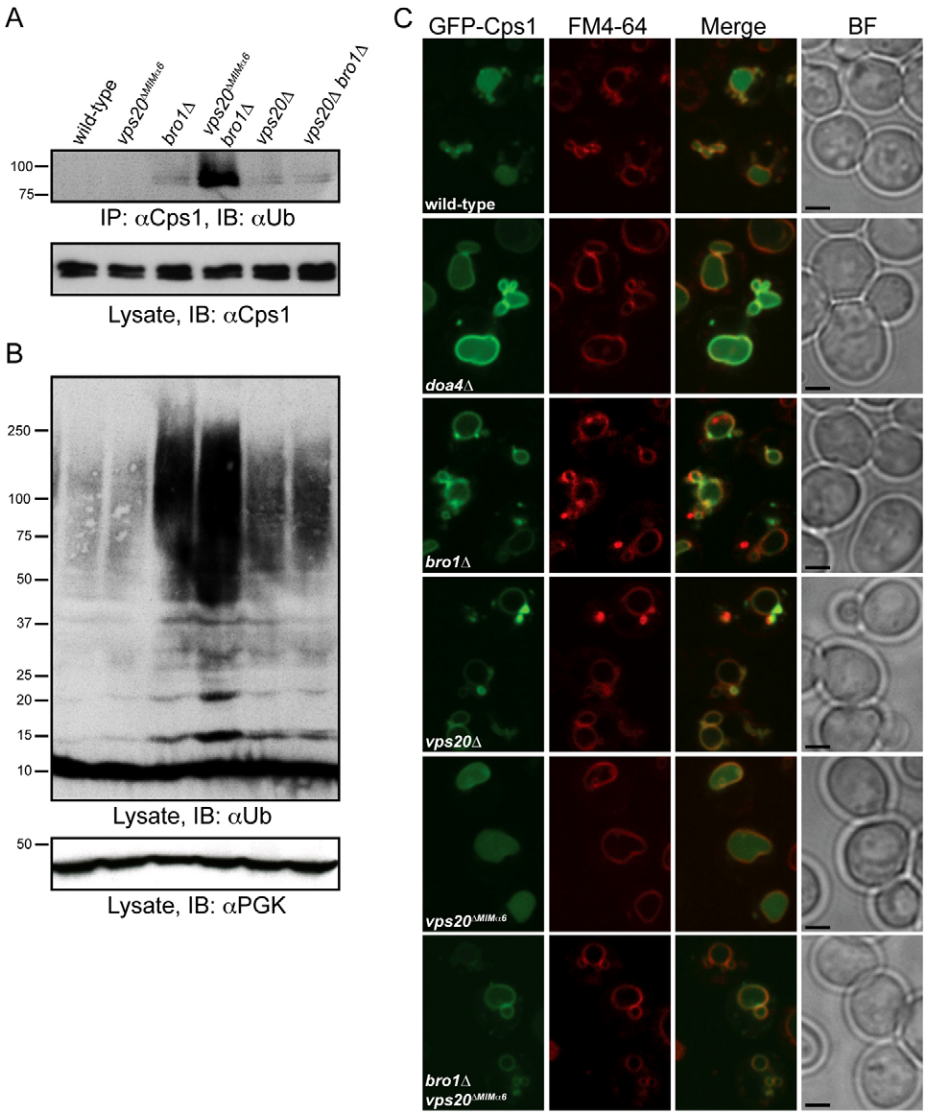

Fig. 4. Mutation of Vps20 MIMα6 exacerbates deubiquitination defects in *bro1Δ* cells. (**A**) Upper panel: Cps1 immunoprecipitations (IP) followed by αUb immunoblotting (IB). Lower panel: αCps1 immunoblotting of whole-cell lysates. (**B**) Immunoblot of whole-cell lysates with αUb and αPGK. (**C**) Fluorescence and brightfield (BF) microscopy of GFP-Cps1 and FM4-64. Scale bars: 2 μm.

Bro1 must have the predominant role in this regard since the *vps20*$^{\Delta MIM\alpha6}$ mutation alone caused no apparent loss of Doa4 Ub hydrolase activity *in vivo*. This conclusion was further supported by the correct localization of GFP-Cps1 in the vacuole lumen in *vps20*$^{\Delta MIM\alpha6}$ mutant cells, which contrasted with the mislocalization of GFP-Cps1 to the vacuole membrane that occurs upon loss of Doa4 function (Katzmann et al., 2001; Fig. 4C). In *bro1Δ* cells and *vps20Δ* cells, GFP-Cps1 was mislocalized both to the vacuole membrane and class E compartments (Odorizzi et al., 2003; Fig. 4C). GFP-Cps1 was similarly mislocalized to the vacuole membrane in *vps20*$^{\Delta MIM\alpha6}$ *bro1Δ* cells, but class E compartments were less prominent in this strain (Fig. 4C), suggesting this aberrant endosomal morphology in *bro1Δ* cells is suppressed by the *vps20*$^{\Delta MIM\alpha6}$ mutation.

Mutation of Vps20 MIMα6 rescues ILV formation in *bro1Δ* cells

The class E compartments formed upon deleting *BRO1* or other ESCRT genes are tubular and cisternal endosomes in which ILVs are largely absent (Odorizzi et al., 2003; Fig. 5A). However, overexpression of the *DOA4* gene in *bro1Δ* cells suppresses class E compartment formation and restores the normal MVB morphology of endosomes (Luhtala and Odorizzi, 2004), raising the possibility that Doa4 promotes ILV formation in a manner that compensates for the absence of Bro1. We speculated such a role for Doa4 might involve Vps20 MIMα6 based on the apparent lack of class E compartment puncta in *vps20*$^{\Delta MIM\alpha6}$ *bro1Δ* cells observed by fluorescence microscopy (Fig. 4C). Therefore, we used electron tomography to determine if the *vps20*$^{\Delta MIM\alpha6}$ mutation has an effect on endosomal morphology.

Mutation of Vps20 MIMα6 alone did not inhibit ILV budding because *vps20*$^{\Delta MIM\alpha6}$ cells had MVBs morphologically similar to those in wild-type yeast (Fig. 5A). However, the class E compartment morphology in *bro1Δ* cells (Fig. 5A,B) was strongly suppressed by introduction of the *vps20*$^{\Delta MIM\alpha6}$ mutation: class E compartments were largely absent in *vps20*$^{\Delta MIM\alpha6}$ *bro1Δ* cells, while spherical MVBs and vesicular tubular endosomes (VTEs) were abundant (Fig. 5A,B). The ILVs present in both *vps20*$^{\Delta MIM\alpha6}$ and *vps20*$^{\Delta MIM\alpha6}$ *bro1Δ* cells had average diameters indistinguishable from those of wild-type cells (Fig. 5C). The *vps20*$^{\Delta MIM\alpha6}$ mutation did not generally suppress class E compartment formation and rescue MVB morphology

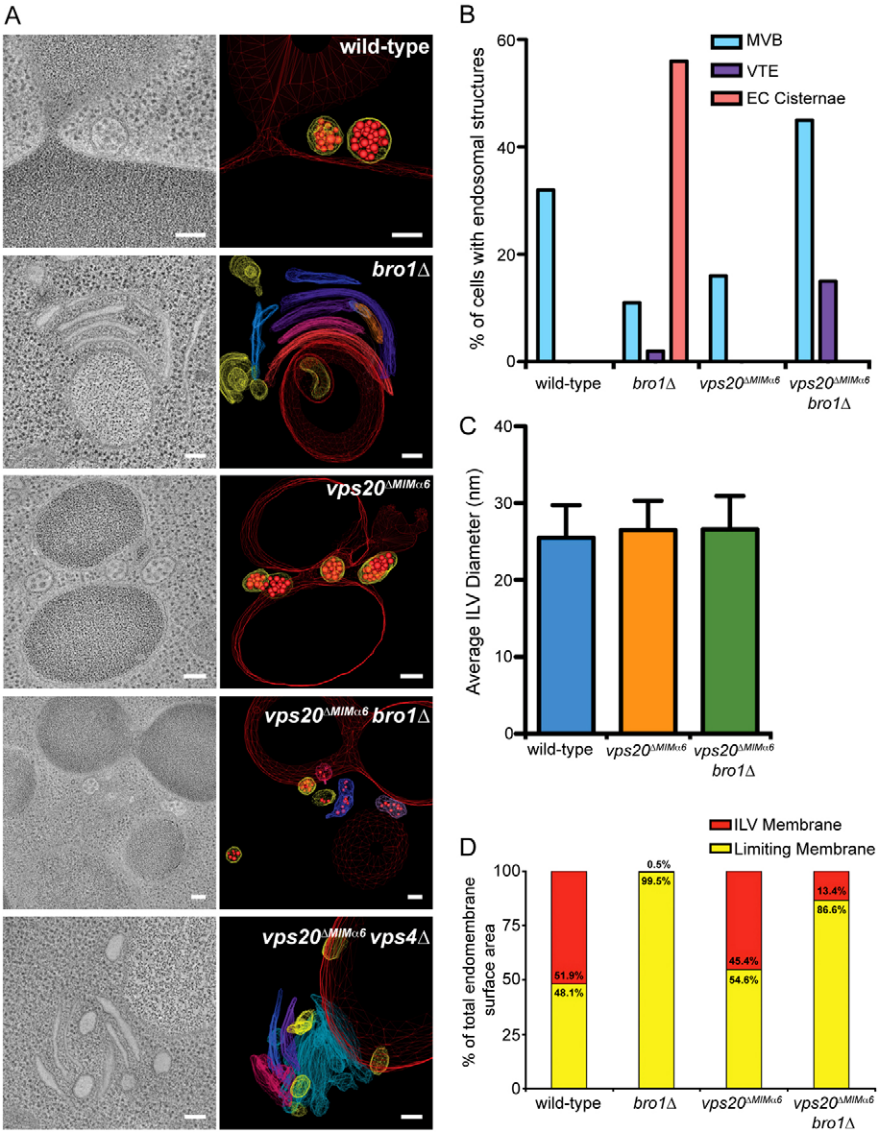

Fig. 5. Mutation of Vps20 MIMα6 rescues ILV budding defects in *bro1Δ* cells. (**A**) Electron tomograms and corresponding models of the indicated strains. In models, ILVs are represented with small red spherical membranes and surrounded by yellow limiting membrane of spherical MVBs. Limiting membranes of tubular MVBs and individual cisternae of the class E compartments are shown in various colors; vacuoles are shown as large red membranes. Scale bars: 100 nm. (**B**) Quantification of the frequency of three endosomal morphologies: multivesicular body (MVB), vesicular tubular endosome (VTE), and class E compartment (EC) cisternae from random planes of 100 cells using transmission electron microcopy (TEM) of 80-nm thin sections of each indicated strain. (**C**) Quantification of average ILV diameters in each indicated strain. Error bars represent ±s.d. (**D**) Quantification of the relative percentages of membrane surface areas within ILVs and limiting membranes in each indicated strain. *vps20*$^{\Delta MIM\alpha 6}$ *vps4Δ* cells exclusively contained class E compartment cisternae without ILVs so were not included in the quantifications in (B–D).

because *vps20*$^{\Delta MIM\alpha 6}$ *vps4Δ* cells had class E compartments and lacked MVBs (Fig. 5A). Despite the rescue of MVB morphology in *vps20*$^{\Delta MIM\alpha 6}$ *bro1Δ* cells, ILVs sparsely filled the lumenal space (Fig. 5A), comprising only ~13% of the total endosomal membrane surface area (Fig. 5D). In contrast, ILVs in MVBs of *vps20*$^{\Delta MIM\alpha 6}$ cells accounted for 45% of endosomal membrane surface area, which is similar to that observed in wild-type yeast (Fig. 5D) and is consistent with Bro1 being required for maximal ILV budding efficiency (Wemmer et al., 2011).

Although the modest recovery in ILV budding in *bro1Δ* cells upon introduction of the *vps20*$^{\Delta MIM\alpha 6}$ mutation might explain why GFP-Cps1 mislocalized to the vacuole membrane under these conditions (Fig. 4C), Cps1 deubiquitination is a prerequisite for the sorting of Cps1 into ILVs (Nikko and André, 2007) and is potently inhibited in *vps20*$^{\Delta MIM\alpha 6}$ *bro1Δ* cells (Fig. 4A). Therefore, we also examined the localization of Sna3, which is an ILV cargo that does not require Doa4 to be sorted into ILVs (Reggiori and Pelham, 2001). Like GFP-Cps1, however, Sna3-GFP failed to be sorted into the vacuole lumen in *vps20*$^{\Delta MIM\alpha 6}$ *bro1Δ* cells (Fig. 6), indicating that the recovery in ILV budding in *bro1Δ* cells upon introduction of the *vps20*$^{\Delta MIM\alpha 6}$ mutation is not sufficient to rescue the sorting of ILV cargoes to the vacuole lumen, regardless of whether these cargoes require deubiquitination to be sorted into ILVs.

Doa4 is required for the rescue of ILV budding in *vps20*$^{\Delta MIM\alpha 6}$ *bro1Δ* cells

The suppression of class E compartment formation and rescue of MVB morphology in *bro1Δ* cells upon mutation of the Doa4-binding site in Vps20 (Fig. 5A) or upon overexpression of the *DOA4* gene (Luhtala and Odorizzi, 2004) suggested that Vps20 MIMα6 inhibits an unknown function for Doa4 in promoting ILV budding in the absence of Bro1. Indeed, the deletion of *DOA4* in *vps20*$^{\Delta MIM\alpha 6}$ *bro1Δ* cells abrogated MVB biogenesis and resulted almost exclusively in class E compartments (Fig. 7A,B). Expression of wild-type *DOA4* from a low-copy plasmid in *vps20*$^{\Delta MIM\alpha 6}$ *bro1Δ doa4Δ* cells restored MVBs and suppressed class E compartments (Fig. 7A,B), confirming that Doa4 is required for the *vps20*$^{\Delta MIM\alpha 6}$ mutation to rescue ILV budding in *bro1Δ* cells. Surprisingly, the Doa4-dependent rescue of ILV

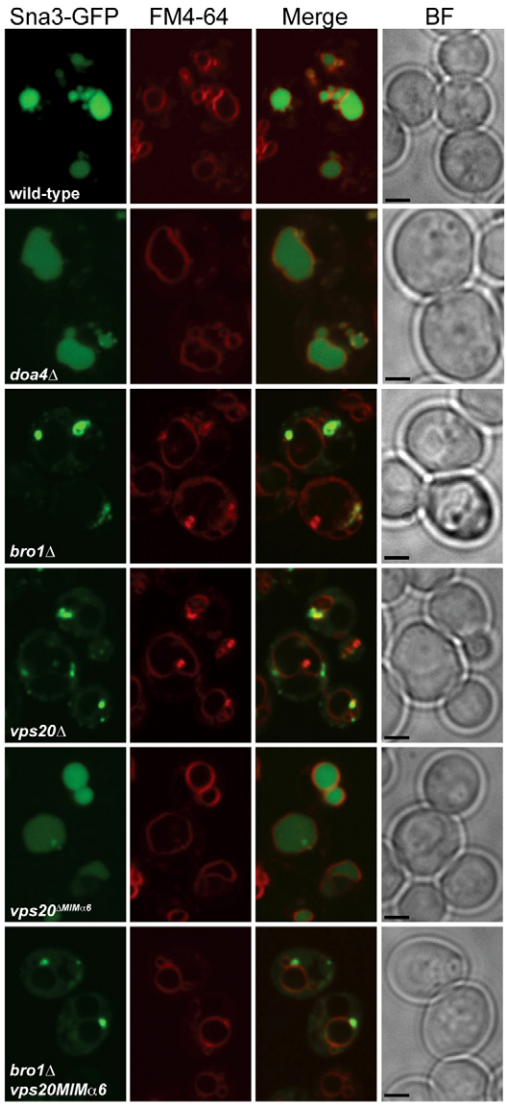

Fig. 6. Mutation of Vps20 MIMα6 does not restore ILV sorting of Sna3-GFP. Fluorescence and brightfield (BF) microscopy of Sna3-GFP and FM4-64. Scale bars: 2 μm.

budding did not require its Ub hydrolase activity, as plasmid-borne expression of the catalytically inactive *doa4*^{C571S} allele also rescued MVB biogenesis in *vps20*$^{\Delta MIM\alpha6}$ *bro1Δ doa4Δ* cells (Fig. 7A,B). Thus, the interaction of Vps20 MIMα6 with the N-terminal domain of Doa4 inhibits a non-catalytic function for Doa4 in promoting ILV budding.

Discussion

Disassembly of ESCRT-III relies on Vps4 and its cofactor, Vta1, both of which contain MIT domains that interact with MIMs at or near the C termini of ESCRT-III subunits (Kieffer et al., 2008; Obita et al., 2007; Stuchell-Brereton et al., 2007). Beyond the Vps4–Vta1 complex, however, no MIT-containing ESCRT-III-associated proteins have been discovered in yeast, despite the abundance of human MIT proteins that are essential for ESCRT-III function in MVB sorting, retroviral budding, and cytokinesis (Kieffer et al., 2008; Renvoisé et al., 2010; Row et al., 2007). The N-terminus of the Doa4 Ub hydrolase in yeast is predicted to have the α-helical structure common to MIT domains, and we found that this region binds directly to a MIM1-like motif in helix α6 (MIMα6) of the Vps20 subunit of ESCRT-III. Although we speculate that the Doa4 N-terminus comprises an MIT domain, structural studies will be required to test this hypothesis.

The most surprising result from our study is that the *vps20*$^{\Delta MIM\alpha6}$ mutation that disables binding of Vps20 to the Doa4 N-terminus rescued ILV budding to a modest extent in *bro1Δ* cells. That ILV biogenesis in *vps20*$^{\Delta MIM\alpha6}$ *bro1Δ* cells was entirely dependent upon *DOA4* expression argues that ILV budding was rescued specifically because Vps20 could not bind Doa4. While it is possible that another protein might also bind Vps20 MIMα6, mutation of this site alone had no apparent effect on endosome morphology or ILV cargo sorting. The requirement for *DOA4* expression to rescue ILV budding in *vps20*$^{\Delta MIM\alpha6}$ *bro1Δ* cells is also inconsistent with a model in which Doa4 antagonizes Vps20 activation of ESCRT-III assembly (Saksena et al., 2009). These findings suggest, instead, that Doa4 has a positive role in ILV budding that is inhibited by its interaction with Vps20. The Doa4–Vps20 interaction might, therefore, constitute a checkpoint that governs the timing of ILV scission in coordination with release of Doa4 from its inhibitory interaction with Vps20. Such a function for Doa4 is unexpected given that, by itself, deletion of the *DOA4* gene does not block ILV biogenesis (Richter et al., 2007). The function of Doa4 that promotes ILV budding must, therefore, be redundant to some extent.

That expression of the catalytically inactive *doa4*^{C571S} allele rescued MVB biogenesis as effectively as did expression of wild-type *DOA4* in *vps20*$^{\Delta MIM\alpha6}$ *bro1Δ* cells indicates that the function of Doa4 that promotes ILV budding does not involve Doa4 Ub hydrolase activity. Current models of ILV budding posit that Vps20 seeds the polymerization of Snf7 into fibrils that are remodeled by Vps24 and Vps2 into helices that promote membrane deformation and scission (Henne et al., 2012; Saksena et al., 2009; Teis et al., 2008). In this light, a mechanism by which Doa4 promotes ILV budding might be through Doa4 contributing to the assembly or remodeling of ESCRT-III oligomers into a scission-competent state. Alternatively, Doa4 might regulate ESCRT-III association with Vps4 to influence the timing of complex disassembly, an idea supported by observation that the MIT domain of AMSH in humans competes with VPS4 for binding to CHMP1B (Agromayor and Martin-Serrano, 2006).

The rescue of MVB biogenesis by the *vps20*$^{\Delta MIM\alpha6}$ mutation in *bro1Δ* but not in *vps4Δ* cells indicates that the liberation of Doa4 from its interaction with Vps20 cannot rescue ILV budding in the face of general ESCRT dysfunction. Moreover, the paucity of ILVs in *vps20*$^{\Delta MIM\alpha6}$ *bro1Δ* cells signifies that, despite recovery of the ILV budding mechanism, Bro1 is required for this process to achieve maximal efficiency. Binding of Bro1 to the Snf7 subunit of ESCRT-III stabilizes the complex by preventing its disassembly, which affects the efficiency with which ILV scission occurs (Wemmer et al., 2011). However, it is unclear whether Doa4 can substitute for Bro1 in this capacity. We detected no direct interaction between the Doa4 N-terminal domain and Snf7 *in vitro*, but the possibility that another region of Doa4 is capable of binding Snf7 is supported by the interaction between full-length Doa4 and Snf7 in a yeast two-hybrid assay (Bowers et al., 2004).

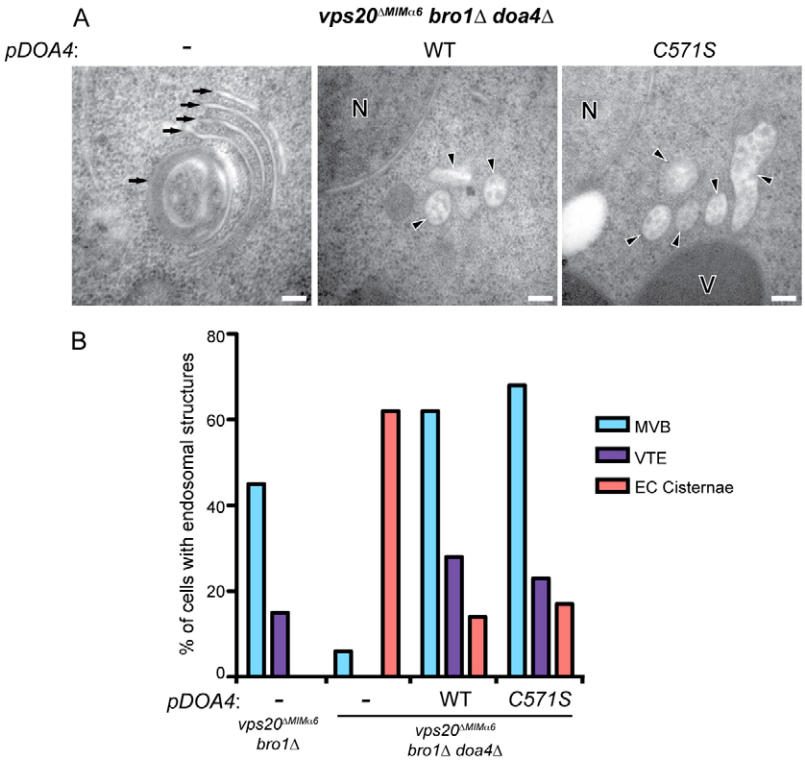

Fig. 7. Rescue of ILV budding in *vps20*$^{\Delta MIM\alpha 6}$ *bro1Δ* cells requires DOA4 expression. (**A**) 80-nm thin section transmission electron micrographs (TEM) of the indicated strains with or without a plasmid expressing wild-type *DOA4* or *doa4*^{C571S}. Arrows and arrowheads indicate class E compartment cisternae and multivesicular bodies, respectively. N, nucleus; V, vacuole. Scale bars: 100 nm. (**B**) Quantification of the frequency of three endosomal morphologies: multivesicular body (MVB), vesicular tubular endosome (VTE), and class E compartment (EC) cisternae from random planes of 100 cells using TEM as in A.

The ATPase activity of human VPS4A is stimulated *in vitro* by its interactions with ESCRT-III subunits, which is predicted to induce a structural rearrangement in VPS4A that prevents the MIT domain and nearby linker region from auto-inhibiting the active site (Merrill and Hanson, 2010). Based on our finding that mutation of the Doa4 binding site in Vps20 exacerbates the deubiquitination defect observed in cells that lack Bro1, Vps20 might have a role in the activation of Doa4. Such a function for Vps20, however, must be secondary to the direct activation of Doa4 Ub hydrolase activity by Bro1 (Richter et al., 2007) because deubiquitination of Cps1, a Doa4 substrate, was unaffected in *vps20*$^{\Delta MIM\alpha 6}$ cells that express Bro1.

MIT domains in two human Ub hydrolases, UBPY and AMSH, mediate recruitment to sites of ESCRT-III assembly (Row et al., 2007; Solomons et al., 2011). However, we found no evidence that the MIT-like N-terminal domain of Doa4 serves the same role because this region alone was not efficiently recruited to endomembranes, and mutation of its binding site in Vps20 did not disable endosomal localization of wild-type Doa4. Nonetheless, we found the N-terminal domain is required for Doa4 endomembrane recruitment, which is consistent with earlier work showing that mutations within this region disrupted Doa4 localization (Amerik et al., 2006) and suggests that amino acids 1-80 are part of a larger endosomal localization

Table 1. Yeast strains used in this study

Strain	Genotype	Reference
SEY6210	MAT-alpha *leu2-3,112 ura3-52 his3Δ200 trp1-Δ901 lys2-Δ801 suc2-Δ9*	Robinson et al., 1988
GOY74	SEY6210; *DOA4-GFP::HIS3MX6*	Luhtala and Odorizzi, 2004
GOY75	SEY6210; *DOA4-GFP::HIS3MX6 vps4Δ::TRP1*	Luhtala and Odorizzi, 2004
GOY23	SEY6210; *pep4Δ::LEU2 prb1Δ::LEU2*	Luhtala and Odorizzi, 2004
DBY5	SEY6210; *doa4Δ::HIS3*	Richter et al., 2007
GOY65	SEY6210; *bro1Δ::HIS3*	Luhtala and Odorizzi, 2004
MBY3	SEY6210; *vps4Δ::TRP1*	Babst et al., 1998
DBY19	GOY23; *vps4Δ::TRP1*	Nickerson et al., 2006
DBY43	GOY23; *bro1Δ::HIS3*	Odorizzi et al., 2003
DBY44	GOY23; *bro1Δ::HIS3 vps4Δ::TRP1*	Odorizzi et al., 2003
GOY248	SEY6210; *vps20*$^{\Delta MIM\alpha 6}$*::KANMX6*	This study
GOY249	GOY248; *vps4Δ::TRP1*	This study
GOY250	GOY65; *vps20*$^{\Delta MIM\alpha 6}$*::KANMX6*	This study
GOY307	SEY6210; *vps20*$^{\Delta MIM\alpha 6}$*::KANMX6 bro1Δ::TRP1 doa4Δ::HIS3MX6*	This study
GOY312	GOY23; *vps20*$^{\Delta MIM\alpha 6}$*::KANMX6*	This study
GOY311	DBY43; *vps20*$^{\Delta MIM\alpha 6}$*::KANMX6*	This study
EEY2-1	SEY6210; *vps20Δ::HIS3*	Babst et al., 2002
GOY314	GOY23; *vps20Δ::HIS3MX6*	This study
GOY315	DBY43; *vps20ΔKANMX6*	This study

domain. Although the N-terminal domain is insufficient for robust endosomal localization of Doa4, the presence of GFP-Doa4$^{1-80}$ in the vacuole lumen of wild-type cells suggests that this domain, when expressed alone, transiently associates with ESCRTs but lacks the ability to be released back into the cytoplasm before its enclosure within an ILV.

That the binding of its N-terminus to Vps20 does not localize Doa4 to endosomes but, instead, inhibits Doa4 function in the formation of ILVs suggests that the Vps20–Doa4 interaction serves as a checkpoint in the ILV budding pathway. Further study is needed to validate the concept of a checkpoint involving this interaction, to establish the time at which Vps20 inhibits Doa4 relative to ESCRT-III assembly, and to identify the mechanism that normally relieves this inhibition.

Materials and Methods

Yeast strains and plasmid construction

Standard techniques were used for growth and genetic manipulation of *S. cerevisiae*. Yeast strains created for this study (Table 1) were constructed using integration cassettes described in Longtine et al. (Longtine et al., 1998). Construction of plasmids expressing GST-Bro1$^{1-387}$ (Kim et al., 2005), 2μ GFP, 2μ GFP-Cps1 (Odorizzi et al., 1998), *DOA4*, and *doa4^{C571S}* (Richter et al., 2007) have been described previously. To construct 2μ *DOA4-GFP*, a PCR product corresponding to the *DOA4-GFP* locus from GOY74 (Luhtala and Odorizzi, 2004) was subcloned into pRS426, resulting in pCR142. To construct 2μ *GFP-DOA4$^{1-80}$* and 2μ *DOA4$^{Δ1-80}$*, PCR products corresponding to *DOA4* codons 1-80 or *DOA4* codons 81-926, respectively, were subcloned into pGO35 (Odorizzi et al., 1998), resulting in pGO640 and pGO704, respectively. To construct *GST-DOA4$^{1-80}$*, a PCR product corresponding to *DOA4* codons 1-80 was cloned into pCR2.1, yielding pCR149, and the *Bam*HI/*Xho*I fragment of pCR149 was subcloned into pGEX-4T1, yielding pCR152. A PCR product corresponding to *VPS2* was cloned into pCR2.1, yielding pGO480. Site-directed mutagenesis was used to create *Sna*BI sites flanking the *VPS2* intron, yielding pGO497, which was then digested with *Sna*BI and re-ligated to make pGO503. The *Xba*I/*Bam*HI fragment of pGO503 was subcloned into the bacterial expression vector pST39 (Tan, 2001) to create pGO516. To construct SNF7 in pST39, pGO465 (Kim et al., 2005) was digested with *Bsp*EI and *Mlu*I to remove *BRO1*, treated with T4 polymerase to generate blunt ends, and re-ligated, yielding pGO547. A PCR product corresponding to *VPS20-HA* was digested with *Sac*I/*Kpn*I and subcloned into pST39, yielding pGO569. To create MIM mutants, Site directed mutagenesis was used on templates pGO516, pGO547, pGO569, and pDN63 (Nickerson et al., 2006) to generate *vps2^{R224D,L225D}* (pCR160), *snf7^{L231D,L234D}* (pGO560), *vps20^{P218D,L219D}-HA* (pCR162), and *His$_6$-vps24^{R218D,L219D}* (pCR161), respectively.

Fluorescence microscopy

Strains were grown to logarithmic phase at 30℃ before observation at room temperature using a Nikon TE2000-U inverted fluorescence microscope equipped with a Yokogawa spinning disc confocal unit (CSU-Xm2; Nikon Instruments, Inc.) and a 100× oil objective with a numerical aperture of 1.4. Fluorescence and brightfield images were acquired with a Photometrics Cascade II EM-CCD camera using MetaMorph (v7.0) software, then processed with ImageJ and Photoshop CS4 software (Adobe). Endosomal membranes were stained with FM4-64 (Molecular Probes, Inc.) using a 20 minute pulse and 90 minute chase (Odorizzi et al., 2003).

Immunoprecipitations and western blotting

For native immunoprecipitations of Doa4-GFP, 20 A_{600} equivalents of logarithmic phase cells were converted to spheroplasts and osmotically lysed and homogenized on ice in 1 ml of lysis buffer (200 mM sorbitol, 50 mM potassium acetate, 20 mM Hepes, pH 7.2, 2 mM EDTA, supplemented with a protease inhibitor cocktail; Roche). Triton X-100 was added to a final concentration of 0.5% and lysates were spun at 16,000 *g* for 10 min at 4℃ to remove insoluble material. One A_{600} equivalent of detergent-soluble lysate was precipitated by the addition of 10% TCA to generate total lysate samples. 10 A_{600} equivalents were incubated with mouse anti-GFP monoclonal antibody (Roche) and Protein G–Sepharose beads (GE Healthcare) for 2 hours at 4℃, after which the beads were collected by centrifugation, washed thrice in lysis buffer, and boiled in Laemmli buffer to elute bound material. Five A_{600} equivalents of immunoprecipitates and 0.5 A_{600} equivalents of total lysate were resolved by SDS-PAGE, transferred to nitrocellulose, and analyzed by western blot using rabbit anti-Bro1, anti-Vps24 and anti-Snf7 polyclonal antiserum (Odorizzi et al., 2003) and mouse anti-GFP (Roche) monoclonal antibody.

Denatured immunoprecipitations to detect Ub-Cps1 were performed as described previously (Katzmann et al., 2001). Twenty A_{600} equivalents of logarithmic phase cells were precipitated by the addition of 10% TCA containing 5 mM *N*-ethylmaleimide (NEM), and whole-cell lysates were generated by glass-bead disruption in lysis buffer (6 M urea, 1% SDS, 50 mM Tris pH 7.5, 1 mM EDTA, 5 mM NEM). Lysates were diluted 10-fold in immunoprecipitation buffer (50 mM Tris pH 7.5, 150 mM NaCl, 0.5% Tween, 1 mM EDTA, 5 mM NEM), insoluble material was cleared by centrifugation at 16,000 *g*, and lysates were immunoprecipitated with anti-Cps1 polyclonal antiserum (Cowles et al., 1997). Five A_{600} equivalents of immunoprecipitates and 0.5 A_{600} equivalents of total lysate were resolved by SDS-PAGE, transferred to nitrocellulose, and analyzed by western blot using anti-Ub (Invitrogen), anti-phosphoglycerate kinase (PGK), and anti-GFP (Roche) monoclonal antibodies (Invitrogen).

Affinity purification of recombinant proteins and *in vitro* binding studies

GST-Doa4$^{1-80}$, GST-Bro1$^{1-387}$, and GST were expressed in *E. coli* BL21-CodonPlus (DE3) cells (Stratagene) by induction with 0.5 mM isopropyl-β-D-thiogalactoside (IPTG) at 20℃ for 18 hours and purified using glutathione–Sepharose (GE Healthcare). Liquid cultures (100 ml) of BL21(DE3) transformed with Vps2, Vps20-HA, His$_6$-Vps24, and Snf7 expression plasmids were grown and lysed as described previously (McNatt et al., 2007). Lysates were clarified of cell debris by centrifugation at 100,000 *g* for 30 min at 4℃. 10 μg of purified GST, GST-Bro1$^{1-387}$, or GST-Doa4$^{1-80}$ was added to 1/3 of each lysate and incubated at 4℃ for 2 hours with glutathione–Sepharose (GE Healthcare). Sepharose was washed 4 times with GST wash buffer [phosphate-buffered saline (PBS), 0.5% Triton X-100] and once with PBS. Samples were resolved by SDS-PAGE, transferred to nitrocellulose, and analyzed by western blot using anti-Vps2, anti-Vps24, and anti-Snf7 polyclonal antiserum (Odorizzi et al., 2003) as well as anti-HA (Covance) and anti-GST (Invitrogen) monoclonal antibodies.

Electron microscopy and tomography

Yeast cells were harvested at log phase, vacuum-filtered on 0.45 micron Millipore paper, loaded into 0.25-mm aluminum planchettes, and high-pressure frozen in a Balzers Bal-Tec HPM 010 (Boeckeler Instruments) as previously described (Wemmer et al., 2011). A Leica AFS (Automated Freeze Substitution, Vienna, Austria) was used for freeze-substitution preparation of 0.1% uranyl acetate and 0.25% glutaraldehyde in anhydrous acetone (Giddings, 2003). Samples were then washed in pure acetone, embedded in Lowicryl HM20 resin (Polysciences, Warrington, PA), and polymerized at −60℃. A Leica Ultra-Microtome was used to cut 80-nm serial thin sections and 250-nm serial semi-thick sections, which were collected onto 1% formvar films, adhered to rhodium-plated copper grids (Electron Microscopy Sciences). A Phillips CM10 (Mahwah, NJ) transmission electron microscope was used to image 80-nm sections at 80 kV to quantify the frequency of MVBs, VTEs, and class E compartments. For tomography, grids were labeled on both sides with fiduciary 15-nm colloidal gold (British Biocell International). Typically, Z-shrinkage of semi-thick sections was 20 percent volume and corrected in final models and measurements. Dual-axis tilt series were collected from ±60° with 1° increments at 200 kV using a Tecnai F20 (FEI-Company, Eindhoven, the Netherlands and Hillsboro, OR) at a magnification of 29,000× using SerialEM (Mastronarde, 2005). 2× binning on the recording 4K × 4K CCD camera (Gatan, Inc., Abingdon, UK) creates a 2K × 2K image with a pixel size of 0.764 nm. Dual-axis electron tomograms (Mastronarde, 1997) of endosomes and ILVs required the IMOD package (Kremer et al., 1996) for tomogram construction and modeling (3DMOD 4.0.11). Manually assigned contours of the endosomal limiting membrane at the inner leaflet were used to measure the surface of the bilayers periodically every 3.85 nm and calculated using imodmesh. Best-fit sphere models were used to measure the diameters of nearly spherical lumenal vesicles from the outer leaflet of the membrane bilayers (O'Toole et al., 2002). IMODINFO provided surface area and volume data of contour models. Data were sorted, analyzed, and graphed using Microsoft Excel and Prism 5.

Acknowledgements

We thank Tess Shideler (University of Colorado) for assistance with fluorescence microscopy and James Hurley (National Institutes of Health) for helpful discussions.

Author contributions

M.W. performed electron microscopy and tomography experiments. All other experiments were performed by C.R.. G.O. and C.R. designed the project, and C.R. wrote the manuscript with comments from co-authors.

Funding

This work was funded by the National Institutes of Health [grant numbers R01GM-065505 and T32GM-08759]. Deposited in PMC for release after 12 months.

References

Agromayor, M. and Martin-Serrano, J. (2006). Interaction of AMSH with ESCRT-III and deubiquitination of endosomal cargo. *J. Biol. Chem.* **281**, 23083-23091.

Amerik, A., Sindhi, N. and Hochstrasser, M. (2006). A conserved late endosome-targeting signal required for Doa4 deubiquitylating enzyme function. *J. Cell Biol.* **175**, 825-835.

Azmi, I., Davies, B., Dimaano, C., Payne, J., Eckert, D., Babst, M. and Katzmann, D. J. (2006). Recycling of ESCRTs by the AAA-ATPase Vps4 is regulated by a conserved VSL region in Vta1. *J. Cell Biol.* **172**, 705-717.

Azmi, I. F., Davies, B. A., Xiao, J., Babst, M., Xu, Z. and Katzmann, D. J. (2008). ESCRT-III family members stimulate Vps4 ATPase activity directly or via Vta1. *Dev. Cell* **14**, 50-61.

Babst, M., Wendland, B., Estepa, E. J. and Emr, S. D. (1998). The Vps4p AAA ATPase regulates membrane association of a Vps protein complex required for normal endosome function. *EMBO J.* **17**, 2982-2993.

Babst, M., Katzmann, D. J., Estepa-Sabal, E. J., Meerloo, T. and Emr, S. D. (2002). Escrt-III: an endosome-associated heterooligomeric protein complex required for mvb sorting. *Dev. Cell* **3**, 271-282.

Bowers, K., Lottridge, J., Helliwell, S. B., Goldthwaite, L. M., Luzio, J. P. and Stevens, T. H. (2004). Protein-protein interactions of ESCRT complexes in the yeast Saccharomyces cerevisiae. *Traffic* **5**, 194-210.

Cowles, C. R., Snyder, W. B., Burd, C. G. and Emr, S. D. (1997). Novel Golgi to vacuole delivery pathway in yeast: identification of a sorting determinant and required transport component. *EMBO J.* **16**, 2769-2782.

Dimaano, C., Jones, C. B., Hanono, A., Curtiss, M. and Babst, M. (2008). Ist1 regulates Vps4 localization and assembly. *Mol. Biol. Cell* **19**, 465-474.

Dupré, S. and Haguenauer-Tsapis, R. (2001). Deubiquitination step in the endocytic pathway of yeast plasma membrane proteins: crucial role of Doa4p ubiquitin isopeptidase. *Mol. Cell. Biol.* **21**, 4482-4494.

Giddings, T. H. (2003). Freeze-substitution protocols for improved visualization of membranes in high-pressure frozen samples. *J. Microsc.* **212**, 53-61.

Henne, W. M., Buchkovich, N. J. and Emr, S. D. (2011). The ESCRT pathway. *Dev. Cell* **21**, 77-91.

Henne, W. M., Buchkovich, N. J., Zhao, Y. and Emr, S. D. (2012). The endosomal sorting complex ESCRT-II mediates the assembly and architecture of ESCRT-III helices. *Cell* **151**, 356-371.

Hurley, J. H. (2010). The ESCRT complexes. *Crit. Rev. Biochem. Mol. Biol.* **45**, 463-487.

Katzmann, D. J., Babst, M. and Emr, S. D. (2001). Ubiquitin-dependent sorting into the multivesicular body pathway requires the function of a conserved endosomal protein sorting complex, ESCRT-I. *Cell* **106**, 145-155.

Kieffer, C., Skalicky, J. J., Morita, E., De Domenico, I., Ward, D. M., Kaplan, J. and Sundquist, W. I. (2008). Two distinct modes of ESCRT-III recognition are required for VPS4 functions in lysosomal protein targeting and HIV-1 budding. *Dev. Cell* **15**, 62-73.

Kim, J., Sitaraman, S., Hierro, A., Beach, B. M., Odorizzi, G. and Hurley, J. H. (2005). Structural basis for endosomal targeting by the Bro1 domain. *Dev. Cell* **8**, 937-947.

Kremer, J. R., Mastronarde, D. N. and McIntosh, J. R. (1996). Computer visualization of three-dimensional image data using IMOD. *J. Struct. Biol.* **116**, 71-76.

Longtine, M. S., McKenzie, A., 3rd, Demarini, D. J., Shah, N. G., Wach, A., Brachat, A., Philippsen, P. and Pringle, J. R. (1998). Additional modules for versatile and economical PCR-based gene deletion and modification in Saccharomyces cerevisiae. *Yeast* **14**, 953-961.

Lottridge, J. M., Flannery, A. R., Vincelli, J. L. and Stevens, T. H. (2006). Vta1p and Vps46p regulate the membrane association and ATPase activity of Vps4p at the yeast multivesicular body. *Proc. Natl. Acad. Sci. USA* **103**, 6202-6207.

Luhtala, N. and Odorizzi, G. (2004). Bro1 coordinates deubiquitination in the multivesicular body pathway by recruiting Doa4 to endosomes. *J. Cell Biol.* **166**, 717-729.

Mastronarde, D. N. (1997). Dual-axis tomography: an approach with alignment methods that preserve resolution. *J. Struct. Biol.* **120**, 343-352.

Mastronarde, D. N. (2005). Automated electron microscope tomography using robust prediction of specimen movements. *J. Struct. Biol.* **152**, 36-51.

McNatt, M. W., McKittrick, I., West, M. and Odorizzi, G. (2007). Direct binding to Rsp5 mediates ubiquitin-independent sorting of Sna3 via the multivesicular body pathway. *Mol. Biol. Cell* **18**, 697-706.

Merrill, S. A. and Hanson, P. I. (2010). Activation of human VPS4A by ESCRT-III proteins reveals ability of substrates to relieve enzyme autoinhibition. *J. Biol. Chem.* **285**, 35428-35438.

Nickerson, D. P., West, M. and Odorizzi, G. (2006). Did2 coordinates Vps4-mediated dissociation of ESCRT-III from endosomes. *J. Cell Biol.* **175**, 715-720.

Nikko, E. and André, B. (2007). Evidence for a direct role of the Doa4 deubiquitinating enzyme in protein sorting into the MVB pathway. *Traffic* **8**, 566-581.

O'Toole, E. T., Winey, M., McIntosh, J. R. and Mastronarde, D. N. (2002). Electron tomography of yeast cells. *Methods Enzymol.* **351**, 81-95.

Obita, T., Saksena, S., Ghazi-Tabatabai, S., Gill, D. J., Perisic, O., Emr, S. D. and Williams, R. L. (2007). Structural basis for selective recognition of ESCRT-III by the AAA ATPase Vps4. *Nature* **449**, 735-739.

Odorizzi, G., Babst, M. and Emr, S. D. (1998). Fab1p PtdIns(3)P 5-kinase function essential for protein sorting in the multivesicular body. *Cell* **95**, 847-858.

Odorizzi, G., Katzmann, D. J., Babst, M., Audhya, A. and Emr, S. D. (2003). Bro1 is an endosome-associated protein that functions in the MVB pathway in Saccharomyces cerevisiae. *J. Cell Sci.* **116**, 1893-1903.

Reggiori, F. and Pelham, H. R. (2001). Sorting of proteins into multivesicular bodies: ubiquitin-dependent and -independent targeting. *EMBO J.* **20**, 5176-5186.

Renvoisé, B., Parker, R. L., Yang, D., Bakowska, J. C., Hurley, J. H. and Blackstone, C. (2010). SPG20 protein spartin is recruited to midbodies by ESCRT-III protein Ist1 and participates in cytokinesis. *Mol. Biol. Cell* **21**, 3293-3303.

Richter, C., West, M. and Odorizzi, G. (2007). Dual mechanisms specify Doa4-mediated deubiquitination at multivesicular bodies. *EMBO J.* **26**, 2454-2464.

Robinson, J. S., Klionsky, D. J., Banta, L. M. and Emr, S. D. (1988). Protein sorting in Saccharomyces cerevisiae: isolation of mutants defective in the delivery and processing of multiple vacuolar hydrolases. *Mol. Cell. Biol.* **8**, 4936-4948.

Rost, B., Yachdav, G. and Liu, J. (2004). The PredictProtein server. *Nucleic Acids Res.* **32 Suppl. 2**, W321-W326.

Row, P. E., Liu, H., Hayes, S., Welchman, R., Charalabous, P., Hofmann, K., Clague, M. J., Sanderson, C. M. and Urbé, S. (2007). The MIT domain of UBPY constitutes a CHMP binding and endosomal localization signal required for efficient epidermal growth factor receptor degradation. *J. Biol. Chem.* **282**, 30929-30937.

Rue, S. M., Mattei, S., Saksena, S. and Emr, S. D. (2008). Novel Ist1-Did2 complex functions at a late step in multivesicular body sorting. *Mol. Biol. Cell* **19**, 475-484.

Saksena, S., Wahlman, J., Teis, D., Johnson, A. E. and Emr, S. D. (2009). Functional reconstitution of ESCRT-III assembly and disassembly. *Cell* **136**, 97-109.

Shestakova, A., Hanono, A., Drosner, S., Curtiss, M., Davies, B. A., Katzmann, D. J. and Babst, M. (2010). Assembly of the AAA ATPase Vps4 on ESCRT-III. *Mol. Biol. Cell* **21**, 1059-1071.

Shim, S., Kimpler, L. A. and Hanson, P. I. (2007). Structure/function analysis of four core ESCRT-III proteins reveals common regulatory role for extreme C-terminal domain. *Traffic* **8**, 1068-1079.

Solomons, J., Sabin, C., Poudevigne, E., Usami, Y., Hulsik, D. L., Macheboeuf, P., Hartlieb, B., Göttlinger, H. and Weissenhorn, W. (2011). Structural basis for ESCRT-III CHMP3 recruitment of AMSH. *Structure* **19**, 1149-1159.

Stuchell-Brereton, M. D., Skalicky, J. J., Kieffer, C., Karren, M. A., Ghaffarian, S. and Sundquist, W. I. (2007). ESCRT-III recognition by VPS4 ATPases. *Nature* **449**, 740-744.

Tan, S. (2001). A modular polycistronic expression system for overexpressing protein complexes in Escherichia coli. *Protein Expr. Purif.* **21**, 224-234.

Teis, D., Saksena, S. and Emr, S. D. (2008). Ordered assembly of the ESCRT-III complex on endosomes is required to sequester cargo during MVB formation. *Dev. Cell* **15**, 578-589.

Vida, T. A. and Emr, S. D. (1995). A new vital stain for visualizing vacuolar membrane dynamics and endocytosis in yeast. *J. Cell Biol.* **128**, 779-792.

Wemmer, M., Azmi, I., West, M., Davies, B., Katzmann, D. and Odorizzi, G. (2011). Bro1 binding to Snf7 regulates ESCRT-III membrane scission activity in yeast. *J. Cell Biol.* **192**, 295-306.

Wollert, T. and Hurley, J. H. (2010). Molecular mechanism of multivesicular body biogenesis by ESCRT complexes. *Nature* **464**, 864-869.

Wollert, T., Wunder, C., Lippincott-Schwartz, J. and Hurley, J. H. (2009). Membrane scission by the ESCRT-III complex. *Nature* **458**, 172-177.

Xiao, J., Xia, H., Zhou, J., Azmi, I. F., Davies, B. A., Katzmann, D. J. and Xu, Z. (2008). Structural basis of Vta1 function in the multivesicular body sorting pathway. *Dev. Cell* **14**, 37-49.